

Keerthy M. Simon · J. M. Chandra Kishen

A multiscale model for post-peak softening response of concrete and the role of microcracks in the interfacial transition zone

Received: 27 May 2017 / Accepted: 5 March 2018 / Published online: 15 March 2018
© Springer-Verlag GmbH Germany, part of Springer Nature 2018

Abstract The effect of microcracks ahead of a macrocrack on the post-peak behavior of concrete-like quasi-brittle material is studied. The critical length of a microcrack is estimated by considering a small element near the macrocrack tip and defining the critical crack opening displacement of the microcrack that exist in the interface region between the aggregate and cement paste. A fracture model is proposed to predict the post-peak response of plain concrete. This model is validated using the experimental results for normal-strength, high-strength and self-consolidating concretes available in the literature. Through a sensitivity analysis, it is observed that the elastic modulus of concrete and the fracture toughness of the interface have a substantial influence on the critical microcrack length.

Keywords Microstructure · Interfacial transition zone · Concrete · Fracture process zone

List of symbols

ITZ	Interfacial transition zone
FPZ	Fracture process zone
ϕ	Airy stress function
$F_n(\theta)$	Eigenfunctions
λ_n	Eigenvalue
μ_{micro}	Shear modulus corresponding to the microscale
ν_{micro}	Poisson's ratio corresponding to the microscale
$K_{\text{Ic}}^{\text{interface}}$	Mode I fracture toughness of interface
$E^{\text{interface}}$	Elastic modulus of interface
d_c	Critical length of microcrack
σ_y	Tensile strength of interface
δ_c	Critical crack opening displacement of microcrack
δ_p	Crack mouth opening displacement corresponding to the peak load
$V_f(\text{ca})$	Volume fraction of coarse aggregate
$V_f(\text{fa})$	Volume fraction of fine aggregate
$V_f(\text{m})$	Volume fraction of mortar
$V_f(\text{cp})$	Volume fraction of cement paste
ν_{eff}	Poissons ratio of concrete

ν_m	Poissons ratio of mortar
E_{ca}	Elastic modulus of coarse aggregate
E_{fa}	Elastic modulus of fine aggregate
E_m	Elastic modulus of mortar
E_{cp}	Elastic modulus of cement paste
V_f	Total volume fraction
m_i	Mass of each constituent
ρ_i	Density of each constituent
D	Depth of specimen
S	Span of the specimen
B	Thickness of the specimen
a	Crack length
a_c	Crack length corresponding to peak load
d_c	Critical microcrack length
δ^M	Crack opening displacement corresponding to peak load
δ^m	Microcrack opening displacement

1 Introduction

Concrete, which is one of the most widely used construction material, is treated as homogeneous from a design perspective. However, on a close meso-level examination it is observed that the internal structure is heterogeneous, consisting of coarse aggregates embedded in cement matrix. Upon magnification of the matrix material, the coexistence of fine aggregate and cement paste can be seen. Further, there exists a region, known as the interfacial transition zone (ITZ) which occurs between the cement paste and aggregates. The cement paste and aggregates are bonded at the interface whose strength depends on its microstructural characteristics.

In fresh concrete, the cement particles cannot pack together efficiently when they are in the close vicinity of a larger object such as aggregate. During the mixing of ingredients to prepare concrete, shearing stresses are exerted on the cement paste by the aggregates. This would lead to the separation of water from cement particles resulting in a region around the aggregate particles with fewer cement particles and is termed as the ITZ [1]. The existence of a thin film of hydrated constituents around the aggregate during hardening of concrete was observed by Farran [1] in 1953. The composition of this zone was found to be different from that of cement paste since the density of cement particles was lower than that of its surroundings. Investigations on the ITZ have shown that its thickness is comparable to the size of cement particles and vary between 20 and 100 μm [2,3]. Although several techniques such as X-ray diffraction, X-ray photoelectron spectroscopy, secondary ion mass spectroscopy, mercury intrusion porosimetry, optical and electron microscopes have been employed to study the ITZ, the complete characterization of the distinctive features of this zone has still not been achieved. The interface acts as a bridge between aggregate and cement paste which neither possesses the properties of aggregate nor the cement paste.

Several investigations have been conducted on concrete to study the development of microcracks and their dependence on the failure mechanisms. Upon loading, microcracking initiates in the ITZ when the local major principal stress exceeds the initial tensile strength of the interface [4]. The development of bond crack along the interface and its dependence on the nonlinear behavior of concrete has been studied by various researchers [5–7] in order to engineer the material for optimal use.

The existence of interfacial transition zone in normal-strength concrete is a well-known fact. Increase in concrete strength can be achieved by reducing porosity, inhomogeneity, and microcracks in the hydrated cement paste and the transition zone. Consequently, there will be reduction in the thickness of the interfacial transition zone in high-strength concrete. The densification of the interfacial transition zone allows for efficient load transfer between the cement mortar and the coarse aggregate, contributing to the strength of the concrete. For very high-strength concrete, wherein the matrix is extremely dense, a coarse aggregate may become the weak link in the corresponding concrete strength. Bentur and Mindless [8] have studied the influence of crack pattern in different types of plain concrete when subjected to bending. They observed that a crack forms around an aggregate particle and propagate along the matrix–aggregate interface in normal-strength concrete. In high-strength concrete, similar observation is seen at lower rate of loading (1 mm/min), whereas, at higher loading rate (250 mm/min) the crack propagates through the aggregate resulting in a shorter crack path.

It is also well known that the fracture behavior of quasi-brittle materials such as concrete is governed by the existence of fracture process zone (FPZ) [9]. The FPZ refers to a region ahead of a macrocrack tip

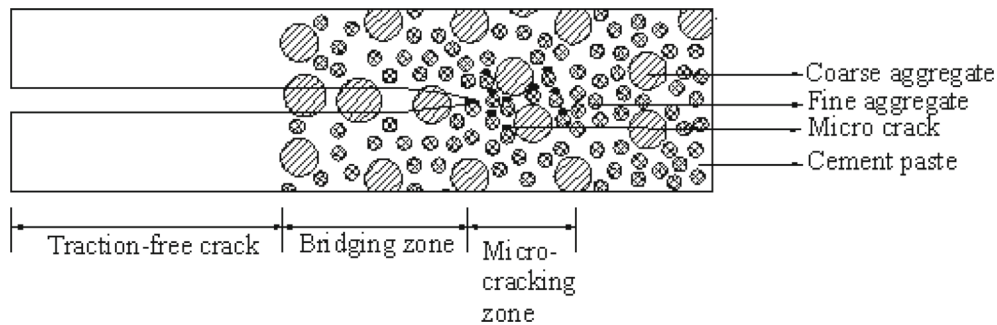


Fig. 1 Fracture process zone

in which various toughening mechanisms such as aggregate bridging, microcracking, crack shielding and crack bridging occur. Nirmalendra and Horri [10] have reported that the major mechanisms responsible for the softening behavior of quasi-brittle materials are microcracking and aggregate bridging as shown in Fig. 1. The bridging zone is assumed to be present around the tip of macrocrack and is followed by large number of microcracks. The restraining stress offered by the bridging zone and the microcracks is responsible for the nonlinear behavior of concrete. The initiation, propagation and coalescence of microcracks within the internal material structure leads to the formation of macrocrack resulting in the softening behavior of the material. The service life of the component can be predicted accurately by considering the effect of restraining stress and microcracks present around the tip of a macrocrack.

When the microcrack reaches a critical length, termed as the critical microcrack length, it propagates and coalesce with other cracks in its vicinity to form a major crack resulting in the failure of the bond. The bond strength at the ITZ is found to have a linear relationship with the concrete strength [11]. The stiffness of the interface decreases although the individual components on either side of the interface possess high stiffness. This is due to the presence of voids and microcracks in this region which do not allow the transfer of stress. The packing and density of the cement particle around the aggregate define the strength of the interfacial zone. The strength of an interface decides whether a crack should grow around an aggregate, or through the aggregate. Also, the fracture energy of the interface is found to be lower than that of the cement paste or an aggregate. The microstructural character of the interfacial zone governs the mode I crack propagation in conventional concrete [12]. Thus, the material behavior of concrete is influenced by the geometry, the spatial distribution and the material property of the individual material constituents and their mutual interaction. Hence, the failure of concrete structures can be viewed as a multiscale phenomenon, wherein, the information of the material properties at a micro-level could be used to determine the system behavior at the macro-level.

In this work, the effects of ITZ and the microcracks on the overall behavior of concrete are studied by estimating the critical length of the microcracks present in the ITZ using the principles of linear elastic fracture mechanics (LEFM). A procedure to determine the material properties at the ITZ including the elastic modulus and the fracture toughness by knowing the mix proportions of the ingredients in concrete is explained. Using the information of the critical microcrack length, an analytical model is proposed through a relationship between the applied stress and the crack opening displacement to obtain the macro-behavior of the material. The proposed model can be used to predict the post-peak response of different mixes of concrete as it accounts for the microstructural properties. The proposed analytical model is validated using experimental results of various investigators that are published in the literature for normal-strength, high-strength and self-consolidating concretes. Furthermore, since various parameters are involved in the determination of the critical microcrack length, which are randomly distributed, an analysis is done to study the most sensitive parameter which affects the microcrack size.

2 Estimation of critical microcrack length

The initiation and propagation of microcrack at the interface between the cement paste and the aggregates are attributed to the toughness of the interface [13]. In this study, the critical microcrack length is a parameter which is used to characterize the interface. Upon loading, the microcrack will initiate at the interface and later coalesce to form a macrocrack. Microcracks are likely to initiate when the load approximately reaches 70–80% of peak load. Beyond the peak load, a sharp decrease in post-peak response of concrete is observed, which is due to the phenomenon of strain localization [14]. Later, it is observed that new microcracks have

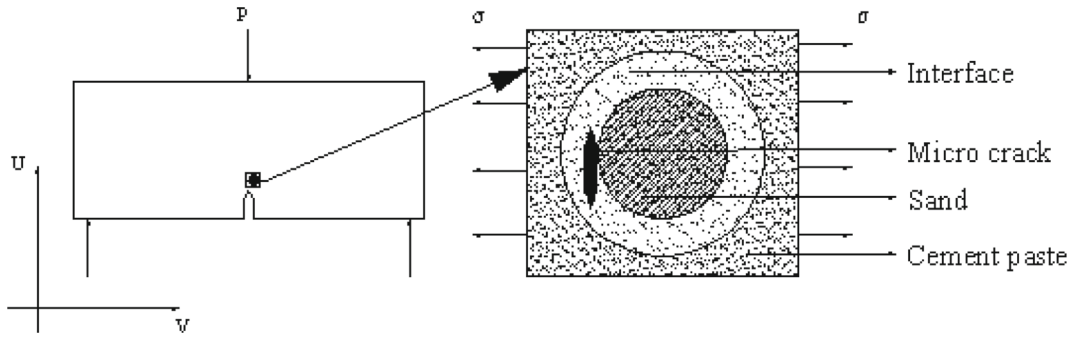


Fig. 2 Representation of microcrack at interface

developed and part of previously developed microcracks are incorporated into macrocrack [15]. In this study, the critical length of the microcrack is determined by analyzing a small element in which the microcrack is likely to occur along the interface between the cement paste and aggregate, existing at the macrocrack tip as depicted in Fig. 2. The interface is considered as a continuous homogeneous medium.

The following assumptions are made: (1) The microcrack is assumed to grow in a direction perpendicular to the maximum principal stress. (2) The initial microcrack length is assumed to be much smaller than the size of the element considered. (3) The microcrack tip is sharp for linear elastic fracture mechanics to be applied.

The stresses and displacement along the crack tip for this two-dimensional crack problem is determined through an inverse method by making use of an Airy stress function (ϕ), which satisfies the biharmonic equation ($\nabla^2 \nabla^2 \phi = 0$). For the problem considered, the Airy stress function which is used to define the stresses and displacement at the microcrack tip is given by [16]

$$\phi = \sum_{n=0}^{\infty} r^{\lambda_n+1} F_n(\theta) \quad (1)$$

where λ_n are the eigenvalues and $F_n(\theta)$ are the corresponding eigenfunctions. Solving the biharmonic equation after substituting Eq. (1) into the same yields the eigenfunction given by.

$$F_n(\theta) = A_n \sin(\lambda_n + 1)\theta + B_n \cos(\lambda_n + 1)\theta + C_n \sin(\lambda_n - 1)\theta + D_n \cos(\lambda_n - 1)\theta \quad (2)$$

For Mode I crack problems, the Airy stress function is an even function of θ . The constants A_n and C_n become zero and the Airy stress function can be written as,

$$\phi = \sum_{n=0}^{\infty} [B_n \cos(\lambda_n + 1)\theta + D_n \cos(\lambda_n - 1)\theta] \quad (3)$$

By making use of the above function, the stresses in the polar coordinate system is determined as

$$\begin{aligned} \sigma_{rr} &= \sum_{n=0}^{\infty} \lambda_n r^{\lambda_n-1} [B_n(\lambda_n + 1)\cos(\lambda_n + 1)\theta + D_n(\lambda_n - 3)\cos(\lambda_n - 1)\theta] \\ \sigma_{\theta\theta} &= \sum_{n=0}^{\infty} \lambda_n r^{\lambda_n-1} [B_n \cos(\lambda_n + 1)\theta + D_n \cos(\lambda_n - 1)\theta] \\ \sigma_{r\theta} &= \sum_{n=0}^{\infty} \lambda_n r^{\lambda_n-1} [B_n(\lambda_n + 1)\sin(\lambda_n + 1)\theta + D_n(\lambda_n - 1)\sin(\lambda_n - 1)\theta] \end{aligned} \quad (4)$$

The corresponding strains are estimated by making use of the stress–strain relationship. Using these strains, the displacements in the polar coordinate system are obtained as

$$\begin{aligned} V_r &= \frac{1}{2\mu_{\text{micro}}} \sum_{n=0}^{\infty} r^{\lambda_n} \left[-(\lambda_n + 1)B_n \cos(\lambda_n + 1)\theta + D_n \cos(\lambda_n - 1)\theta \left\{ \frac{4}{1 + \nu_{\text{micro}}} - (\lambda_n + 1) \right\} \right] \\ V_\theta &= \frac{1}{2\mu_{\text{micro}}} \sum_{n=0}^{\infty} r^{\lambda_n} \left[-(\lambda_n + 1)B_n \sin(\lambda_n + 1)\theta + D_n \sin(\lambda_n - 1)\theta \left\{ \frac{4}{1 + \nu_{\text{micro}}} + (\lambda_n - 1) \right\} \right] \end{aligned} \quad (5)$$

In the above equations, μ_{micro} and ν_{micro} are the shear modulus and the Poisson's ratio of the interface, respectively, where the microcrack is likely to occur. The microcrack present in the interface is assumed to be sharp in order to initiate the crack propagation. The crack surfaces of the microcrack are considered as stress free and the corresponding boundary condition along the upper surface denoted by (+) and lower surface (−) is given by Eq. (6). The stresses need to satisfy the traction free boundary condition along the microcrack surface.

$$\sigma_{\theta\theta} = \sigma_{r\theta} = 0, \quad \theta = \pm\pi \quad (6)$$

Substituting the micro-stress fields given by Eq. (4) into the boundary condition leads to the characteristic equation $\lambda_1 \sin(2\beta^*) + \sin(2\lambda_1\beta^*) = 0$. Assuming the microcrack to be very sharp, the microcrack angle attains a value of π and the characteristic equation reduces to $\sin(2\lambda_n\pi) = 0$. The roots of this characteristic equation give the eigenvalue ($\lambda_n = \frac{n}{2}$; $n = 0 \pm 1 \pm 2, \dots$). The crack tip singularity is observed when the eigenvalue becomes 0.5. The displacement field near the microcrack tip reduces to the following form

$$\begin{aligned} V_r &= \frac{r^{1/2}}{2\mu_{\text{micro}}} \left[-\left(\frac{1}{2} + 1\right) B_1 \cos\left(\frac{1}{2} + 1\right)\theta - \left(\frac{1}{2} + 1\right) D_1 \cos\left(\frac{1}{2} - 1\right)\theta \right. \\ &\quad \left. + \left(\frac{4}{1 + \nu_{\text{micro}}}\right) D_1 \cos\left(\frac{1}{2} - 1\right)\theta \right] \end{aligned} \quad (7)$$

$$\begin{aligned} V_\theta &= \frac{r^{1/2}}{2\mu_{\text{micro}}} \left[\left(\frac{1}{2} + 1\right) B_1 \sin\left(\frac{1}{2} + 1\right)\theta + \left(\frac{1}{2} - 1\right) D_1 \sin\left(\frac{1}{2} - 1\right)\theta \right. \\ &\quad \left. + \left(\frac{4}{1 + \nu_{\text{micro}}}\right) D_1 \sin\left(\frac{1}{2} - 1\right)\theta \right] \end{aligned} \quad (8)$$

A relationship between B_1 and D_1 is obtained by substituting the eigenvalue into the boundary condition ($B_1 = D_1/3$). This reduces the displacement field in terms of one unknown parameter D_1 . Further, by defining $D_1 = K_1/\sqrt{2\pi}$, the displacement field becomes a function of stress intensity factor (K). The microcrack opening displacement is derived by transforming the displacements to the rectangular coordinate, by making use of the relation $V^+ = V_r \sin\pi + V_\theta \cos\pi$ and $V^- = -V_r \sin\pi + V_\theta \cos\pi$, where V^+ and V^- represent the displacement along the upper and lower crack surface in the direction perpendicular to loading. The microcrack opening displacement (δ^{micro}) is given by

$$\delta^{\text{micro}} = V^+ - V^- = 8\sqrt{\frac{r}{2\pi}} \frac{K}{E} \quad (9)$$

As the microcrack initiates in the interfacial region, the stress intensity factor K , elasticity modulus E and r are replaced with $K^{\text{Interface}}$, $E^{\text{Interface}}$ and $d/2$ (as the total length of microcrack is assumed to be d). When the microcrack reaches a critical length (i.e., $d = d_c$), the corresponding fracture toughness and crack opening displacement reach their critical value ($K_{\text{Ic}}^{\text{Interface}}$, δ_c) and are given by,

$$\delta_c^{\text{micro}} = 4\sqrt{\frac{d_c}{\pi}} \frac{K_{\text{Ic}}^{\text{interface}}}{E^{\text{Interface}}} \quad (10)$$

When the applied load reaches the peak load, the microcrack becomes critical and those microcrack which becomes critical will coalesce with the existing macrocrack leading to the propagation of crack. The existence of the microcrack at the macrocrack tip considered in this study is represented by Fig. 3. The macrocrack length and the stress corresponding to the peak load (P_{peak}) are represented as the critical macrocrack length (a_c)

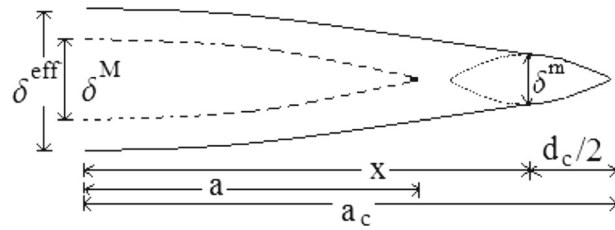


Fig. 3 Representation of COD of macrocrack by considering the effect of microcrack at peak load

and peak stress (σ_p), respectively. The crack length corresponding to the peak load is determined by knowing the crack mouth opening displacement (δ_p) at the peak load. The crack opening displacement at any point (x) along the macrocrack is given by,

$$\delta^{\text{macro}} = \frac{4\sigma_p a_c}{E} g_2\left(\frac{a_c}{b}\right) g_3\left(\frac{x}{a_c}, \frac{a_c}{b}\right) \tag{11}$$

where σ_p is the stress corresponding to the peak load, E is the elastic modulus of concrete, b is the depth of the specimen and the geometric factors $g_2\left(\frac{a_c}{b}\right)$ and $g_3\left(\frac{x}{a_c}, \frac{a_c}{b}\right)$ for specimen with the span $s = 4b$ given by [14]

$$g_2\left(\frac{a_c}{b}\right) = 0.76 - 2.28\left(\frac{a_c}{b}\right) + 3.87\left(\frac{a_c}{b}\right)^2 - 2.04\left(\frac{a_c}{b}\right)^3 + \frac{0.66}{\left(1 - \frac{a_c}{b}\right)^2} \tag{12}$$

$$g_3\left(\frac{x}{a_c}, \frac{a_c}{b}\right) = \sqrt{\left(1 - \frac{x}{a_c}\right)^2 + \left(1.081 - 1.149\frac{a_c}{b}\right) \left\{\frac{x}{a_c} - \left(\frac{x}{a_c}\right)^2\right\}} \tag{13}$$

From Fig. 3, it is clear that the crack opening displacement due to the macrocrack at $(x = a_c - d_c/2)$ will be equal to the crack opening displacement due to the microcrack at $r = d_c/2$. The critical microcrack length is determined by equating both the crack opening displacements given by Eqs. (10) and (11). The solution of the following equation gives the critical microcrack length.

$$\delta^{\text{macro}}|_{x=(a_c - \frac{d_c}{2})} = \delta^{\text{micro}}|_{r=\frac{d_c}{2}} \tag{14}$$

$$\frac{4\sigma_p a_c}{E} g_2\left(\frac{a_c}{b}\right) g_3\left(\frac{x}{a_c}, \frac{a_c}{b}\right) = 4\sqrt{\frac{d_c}{\pi}} \frac{K_{IC}^{\text{interface}}}{E^{\text{Interface}}} \tag{15}$$

As seen from the above equation, the critical microcrack length can be obtained by knowing the fracture toughness and elastic modulus of the interfacial zone. These interfacial properties depend on the mix proportions of ingredients used in the preparation of the concrete. In the next section, a procedure for estimating the interfacial properties which makes use of the mix proportion of the constituents of concrete is explained.

3 Interfacial fracture toughness

The lower density of cement particles around the aggregates makes the interface more prone to cracking. The initiation and propagation of a microcrack depend on the toughness of the interface. Hillemeier and Hilsdorf [17] conducted experiments and analytical investigations to determine the fracture properties of hardened cement paste, aggregate and cement–paste interface. Huang and Li [18] considered the nucleation of a crack along the interface of aggregate and mortar and derived a relation between the effective toughness of the material and the mortar in terms of volume fractions by considering the crack deflection and interfacial cracking effects, which is given by

$$\frac{K_{IC}}{K_{IC}^m} = \sqrt{1 + 0.87(V_f(\text{ca}))} \sqrt{\frac{1}{1 - (\pi^2/16)V_f(\text{ca})(1 - \nu_{\text{eff}}^2)}} \tag{16}$$

where K_{IC} is the fracture toughness of concrete, K_{IC}^m is the fracture toughness of mortar, $V_f(\text{ca})$ is the volume fraction of coarse and ν_{eff} is the Poisson’s ratio of concrete.

In this work, a relation between the toughness of matrix and cement paste is obtained by suitably modifying and replacing the fracture toughness of concrete and mortar with those of mortar and cement paste. Also, the volume fraction of coarse aggregate and Poisson's ratio of concrete is replaced with that of fine aggregate and Poisson's ratio of mortar which takes the form

$$\frac{K_{IC}^m}{K_{IC}^{cp}} = \sqrt{1 + 0.87(V_f(fa))} \sqrt{\frac{1}{1 - (\pi^2/16)V_f(fa)(1 - \nu_m^2)}} \quad (17)$$

Rewriting Eq. (16) in terms of K_{IC}^m and substituting it into Eq. (17) yields a relation between the toughness of concrete and cement paste. The fracture toughness of cement paste–aggregate interface is much lower than that of cement paste. Hillemeier and Hilsdorf [17] conducted experiments to determine the fracture toughness of the interface and the cement paste and observed the toughness of the interface to be 0.4 times of the cement paste (i.e., $K_{IC}^{Interface} = 0.4K_{IC}^{cp}$) which is used in the present study. The fracture toughness of interface takes the form,

$$K_{IC}^{Interface} = \left(\frac{0.4}{\sqrt{1 + 0.87V_f(ca)} \sqrt{\frac{1}{1 - \frac{\pi^2}{16}V_f(ca)(1 - \nu_{ef}^2)}}} \right) \times \left(\frac{K_{IC}}{\sqrt{1 + 0.87V_f(fa)} \sqrt{\frac{1}{1 - \frac{\pi^2}{16}V_f(fa)(1 - \nu_m^2)}}} \right) \quad (18)$$

4 Interfacial elastic modulus

The elastic modulus of the interface is another major parameter used in the definition of the critical microcrack length (d_c) in Eq. (15) and is reported to be 0.7 times the elastic modulus of cement paste (E_{cp}) [19] and adopted in this study. Hashin [20] obtained a relation between the elastic modulus of homogeneous material with and without inclusion, based on volume fraction and modulus of the inclusion by considering the change in the strain energy in a loaded homogeneous body due to the insertion of inhomogeneities using the variational theorems of elasticity. Accordingly, the relation between the elastic modulus of concrete and mortar is expressed as,

$$\frac{E}{E_m} = \frac{V_f(m)E_m + (1 + V_f(ca))E_{ca}}{(1 + V_f(ca))E_m + V_f(m)E_{ca}} \quad (19)$$

where $V_f(m)$ and $V_f(ca)$ are the volume fraction of mortar and coarse aggregate and E , E_m and E_{ca} are the elastic modulus of concrete, mortar and coarse aggregate, respectively. The above equation can be simplified to the form,

$$V_f(m)E_m^2 + [1 + V_f(ca)]E_m[E_{ca} - E] - V_f(m)E_{ca}E = 0 \quad (20)$$

The elastic modulus of the mortar is obtained by solving the above quadratic equation. The relationship between the modulus of elasticity of mortar and cement paste is obtained in a similar manner by replacing the material properties of concrete and mortar with the properties of mortar and cement paste. Also, the volume fraction of coarse aggregate and mortar is replaced with those of fine aggregate and cement paste. The modulus of elasticity of cement paste is finally determined by solving the following quadratic equation.

$$V_f(cp)E_{cp}^2 + [1 + V_f(fa)]E_{cp}[E_{fa} - E_m] - V_f(cp)E_{fa}E_m = 0 \quad (21)$$

where $V_f(cp)$ and $V_f(fa)$ are the volume fraction of cement paste and fine aggregate and E_m , E_{cp} and E_{fa} are the elastic modulus of mortar, cement paste and fine aggregate, respectively.

5 Volume fraction of constituents

It is evident from Eqs. (18), (20) and (21) that the determination of volume fraction of constituents is necessary to compute the fracture toughness and elastic modulus of the interface. Knowing the mix proportion of concrete by weight we can determine the volume fraction of constituents as discussed below. Let m_1, m_2, m_3 and m_4 be the ratio of cement, fine aggregate, coarse aggregate and water in concrete mix by weight. Total mass (m) is the sum of mass of individual constituent times x , where x is the mass of cement. The total volume fraction of all the constituent leads to unity, which can be expressed as,

$$V_f = V_{f1} + V_{f2} + V_{f3} + V_{f4} = \sum_{i=1}^n V_{fi} = 1 \quad (22)$$

where V_{fi} is the volume fraction of each constituent and i varies from 1 to n and n is the number of constituents. The volume fraction of each constituent is defined as the ratio of volume of that particular constituent (V_i) to that of the total volume (V) and is given by,

$$V_{fi} = \frac{V_i}{V} = \frac{(m_i)x}{\rho_i V} \quad (23)$$

where $(m_i)x$ and ρ_i are the mass and density of each constituent, respectively. The total volume of all constituents (V_f) is rewritten in terms of mass and density of each constituent by substituting Eq. (23) into Eq. (22) and is given by,

$$V_f = \sum_{i=1}^n \frac{(m_i)x}{\rho_i V} = 1 \quad (24)$$

The total volume of the constituents can be rewritten in terms of mass and density of each constituents by making use of the above relation.

$$V = \sum_{i=1}^n \frac{(m_i)x}{\rho_i} \quad (25)$$

Substituting Eq. 25 into Eq. 23 the volume fraction of each constituent is obtained as,

$$V_{fi} = \frac{m_i}{\rho_i \left[\sum_{i=1}^n \frac{m_i}{\rho_i} \right]}. \quad (26)$$

6 Post-peak macro-behavior of concrete

In this section, the effects of microcracks on the macro-behavior of plain concrete is studied through its post-peak response. A relationship is obtained between the applied stress (σ) and the crack opening displacement (δ^M) along the failure plane, which occurs due to the propagation of a dominant crack. The energy required to open and propagate a crack could be obtained through the following relationship

$$G = \int_0^{\delta} \sigma d\delta \quad (27)$$

Differentiating the above equation with respect to the crack opening displacement (δ) results in the stress (σ) which upon substituting the relation between G and K_{eff} ($G = K_{\text{eff}}^2/E$) results in

$$\sigma = \frac{1}{E} \frac{d}{d\delta} (K_{\text{eff}}^2) \quad (28)$$

where K_{eff} is the stress intensity at crack tip a as shown in Fig. 3. The micro- and macrocrack profiles at the peak load are represented in Fig. 3. At peak load, the microcrack becomes critical and reaches a length d_c and coalesce with the macrocrack a and the macrocrack corresponding to the peak load is represented as a_c . When

the crack reaches size a as shown in Fig. 3, the corresponding crack mouth opening displacement (CMOD) is given by [14]

$$\delta^{\text{eff}} = \frac{4\sigma a}{E} g_2 \left(\frac{a}{b} \right) \quad (29)$$

The above equation is further modified and expressed in terms of stress intensity factor (SIF) and CMOD as

$$K_{\text{eff}} = \sqrt{\frac{\pi}{a}} \frac{\delta^{\text{eff}} E g_1 \left(\frac{a}{b} \right)}{4g_2 \left(\frac{a}{b} \right)} \quad (30)$$

Substituting Eqs. (30) into (28) yields the following form

$$\sigma = \frac{1}{E} \frac{d}{d\delta} \frac{\pi}{16} \frac{\delta^{\text{eff}2} E^2}{a} \frac{g_1 \left(\frac{a}{b} \right)^2}{g_2 \left(\frac{a}{b} \right)^2} = \frac{\pi}{8} \frac{\delta^{\text{eff}} E}{a} \frac{g_1 \left(\frac{a}{b} \right)^2}{g_2 \left(\frac{a}{b} \right)^2} \quad (31)$$

where δ^{eff} is the crack opening displacement when the macrocrack reaches the length a as shown in Fig. 3. The crack opening displacement corresponding to the peak load (i.e., when the crack reaches a_c) (δ^{M}) can be approximated to the sum of δ^{eff} and the crack opening due to the microcrack (δ^{m}) as depicted in Fig. 3.

$$\delta^{\text{M}} = \delta^{\text{eff}} + \delta^{\text{m}} \text{ or } \delta^{\text{eff}} = \delta^{\text{M}} - \delta^{\text{m}} \quad (32)$$

Replacing δ^{eff} in Eq. (31) by Eq. (32) yields

$$\sigma = \frac{\pi}{8} \frac{E}{a} \frac{g_1 \left(\frac{a}{b} \right)^2}{g_2 \left(\frac{a}{b} \right)^2} (\delta^{\text{M}} - \delta^{\text{m}}) \quad (33)$$

Thus, the crack opening displacement due to the macrocrack takes the form

$$\delta^{\text{M}} = \frac{8}{\pi} \frac{\sigma a}{E} \frac{g_2 \left(\frac{a}{b} \right)^2}{g_1 \left(\frac{a}{b} \right)^2} + \delta^{\text{m}} \quad (34)$$

By substituting $a = (a_c - d_c)$ and also by replacing $a_c = K_{\text{Ic}}^2 / \sigma \pi g_1 \left(\frac{a_c}{b} \right)^2$, the macrocrack opening displacement simplifies to

$$\delta^{\text{M}} = \frac{8}{\pi^2} \frac{K_{\text{Ic}}^2}{E \sigma_p (\sigma / \sigma_p)} \left\{ \frac{g_2 \left(\frac{a_c - d_c}{b} \right)}{g_1 \left(\frac{a_c - d_c}{b} \right) g_1 \left(\frac{a_c}{b} \right)} \right\}^2 \left[1 - \left(\frac{\sigma}{\sigma_p} \right)^2 \frac{\sigma_p^2 d_c \pi}{K_{\text{Ic}}^2} \right] + \delta^{\text{m}} \quad (35)$$

where K_{Ic} is the fracture toughness of the material, d_c is the critical microcrack length and δ^{m} is the microcrack opening displacement when the microcrack becomes critical and is given by Eq. (10). Equation (35) is used to predict the post-peak behavior of concrete.

7 Analysis of experimental data

The interfacial properties such as the modulus of elasticity, fracture toughness and the critical microcrack length as discussed in the previous section are evaluated for five different concretes used by researchers in their respective experimental programs. The following experimental data are considered in this analysis: Bazant and Xu [21], Shah [22], Prasad and Sagar [23], Gettu et al. [24] and Hemalatha et al. [25].

In all the research mentioned above, tests have been carried out on beams of three different sizes (designated as small, medium and large) which are geometrically similar under three-point bending. While in the first three experimental programs mentioned above normal-strength plain concrete have been used, Gettu et al. [24] have used high-strength concrete. Hemalatha et al. [25] have used self-consolidating concrete with two types of mineral admixtures—one containing only fly ash (SCC2) and other with fly ash and silica fumes (SCC3). Table 1 shows the dimensions of the beams, the peak stress, the crack mouth opening displacement (CMOD)

Table 1 Geometry and material properties of specimens

Specimen designation	Depth	Span	Peak stress	CMOD at peak load	Critical CMOD	Fracture toughness	Elastic modulus
	D (mm)	S (mm)	σ_p (N/mm ²)	δ_p (mm)	δ_c (mm)	K_{Ic} (MPa $\sqrt{\text{mm}}$)	E (N/mm ²)
S [22]	76	190	4.476	0.0567	0.490	44.6	30,000
M [22]	152	380	3.589	0.0743	0.570	44.6	30,000
L [22]	304	760	3.338	0.0483	0.872	44.6	30,000
S [21]	38.1	95	4.750	0.0270	0.089	32.0	27,120
M [21]	76.2	191	3.833	0.0354	0.087	32.0	27,120
L [21]	152.4	381	3.364	0.0436	0.075	32.0	27,120
M [24]	76.2	191	3.060	0.0317	0.089	38.0	37,600
L [24]	152.4	38.1	2.460	0.0413	0.100	38.0	37,600
S2 [25]	76	190	2.735	0.0364	0.420	28.2	31,000
M2 [25]	152	380	2.539	0.0391	0.400	28.2	31,000
L2 [25]	304	760	2.085	0.0499	0.660	28.2	31,000
S3 [25]	76	190	3.728	0.0386	0.490	40.0	33,000
M3 [25]	152	380	3.005	0.0500	0.380	40.0	33,000
L3 [25]	304	760	2.990	0.0765	0.690	40.0	33,000
S [23]	80	240	4.650	0.0747	0.580	73.3	44,159
M [23]	160	480	3.611	0.1025	0.680	60.0	44,159
L [23]	320	960	4.048	0.0780	0.730	72.0	44,159

S small, M medium, L large, S2 small (SCC2), M2 medium (SCC2), L2 large (SCC2), S3 small (SCC3), M3 medium (SCC3), L3 large (SCC3)

at peak load, the critical CMOD and material properties including the fracture toughness and elastic modulus as reported in all these experimental work.

As discussed in the previous sections, the interfacial properties of concrete depend on the volume fraction of each of its constituents. Table 2 gives the mix proportions and the volume fractions of the aggregates for the different concretes considered in this study. The interfacial fracture toughness, the interfacial elastic modulus and the critical microcrack length are calculated using Eqs. (15), (18), and (21), respectively, and are tabulated in Table 3. It is seen that the interface is the weaker region and is therefore more prone to cracking and justifies the analysis of the interfacial region. Furthermore, as reported in the literature [14], if the interface is weaker than the coarse aggregates, the crack propagates around the aggregate. Another observation that can be made from Table 3 is that the interfacial elastic modulus of high-strength concrete and self-consolidating concrete is greater than the normal concrete. This is due to the presence of more powder content in these concretes. It is also observed in Table 3 that for a particular concrete mix, the computed interfacial properties remain constant.

The critical microcrack length is found to be dependent on the properties of the interface as well as the geometry of the specimen and is reported in Table 3. Further it is found to increase with the size of the specimen, although the interfacial properties remain the same. Also, Mobasher et al. [26] have reported that 80% of number of microcrack are smaller than 1.5 mm in length. The critical length of microcrack is found to be comparable with the size of the fine aggregate and cement particles. Further, the critical microcrack length is normalized with the depth of beam as shown in Table 3. It is seen that this normalized value remains almost constant for a given mix of concrete and could be treated as a material property.

8 Validation of the proposed model

The model proposed to determine the post-peak macro-behavior of the concrete specimen using the microscopic properties as represented by Eq. (35) is validated for the five different concretes mentioned in the earlier section. This model makes use of the interfacial properties as determined in the previous sections and shown in Table 3. Figures 4, 5 and 6 show the post-peak behavior determined by considering the effect of microcracks for different concretes as predicted by the proposed model. The experimentally obtained results are also superposed on the same plots. These plots are normalized with the peak stress reported in Table 1 for the ordinates and critical crack opening displacement (δ_c) obtained from experiments as reported in Table 1 for the abscissa.

In Fig. 4, the results of normal-strength concrete are presented. The legend in this figure indicates two letters followed by either model or experiment. The first letter (S, M, L) indicates the size (small, medium, large) of the beam specimen and the second letter (B, S) indicates the experimental work of Bazant and Xu [21]

Table 2 Mix proportions and volume fractions of aggregate

Reference proportion	Mix of coarse agg.	Volume fraction	Volume fraction of fine agg.
[22]	1:1.86:2.61:0.54 C:CA:FA:W	0.2	0.44
[21]	1:2:2:0.6 C:CA:FA:W	0.23	0.38
[24]	1:1.35:2.42:0.35:0.25:0.04 C:CA:FA:W:F:MS	0.18	0.49
[25]	1:1.7:1.46:0.46:0.2:0.02 C:CA:FA:W:F:SP	0.22	0.26
[25]	1:1.71:1.4:0.38:0.2:0.1:0.024 C:CA:FA:W:F:SF:SP	0.25	0.27
[23]	1:1.57:2.35:0.34:0.12:0.012 C:CA:FA:W:MS:SP	0.35	0.38

C cement, CA coarse agg., FA fine agg., W water, F fly ash, MS micro-silica, SP super plasticizers, SF silica fumes

Table 3 Interface properties and critical microcrack length

Specimen designation	Fracture toughness $K_{Ic}^{Interface}$ (MPa \sqrt{mm})	Elastic modulus $E^{Interface}$ (N/mm ²)	Microcrack Length d_c (mm)	d_c/D 10 ⁻² –
Small [22]	16.76	5413.5	0.3659	0.42
Medium [22]	16.76	5413.5	0.5717	0.38
Large [22]	16.76	5413.5	0.9238	0.34
Small [21]	12.45	5488.7	0.2370	0.62
Medium [21]	12.45	5488.7	0.4540	0.60
Large [21]	12.45	5488.7	0.9167	0.60
Medium [24]	14.17	8265.5	0.5084	0.66
Large [24]	14.17	8265.5	1.0871	0.70
Small [25]	12.27	6809.3	0.2918	0.38
Medium [25]	12.27	6809.3	0.5902	0.38
Large [25]	12.27	6809.3	1.1832	0.38
Small [25]	16.51	7539.7	0.3880	0.51
Medium [25]	16.51	7539.7	0.7720	0.51
Large [25]	16.51	7539.7	1.6150	0.51
Small [23]	27.01	8194.7	0.3840	0.46
Medium [23]	22.02	8194.7	0.6813	0.42
Large [23]	26.01	8194.7	1.3175	0.41

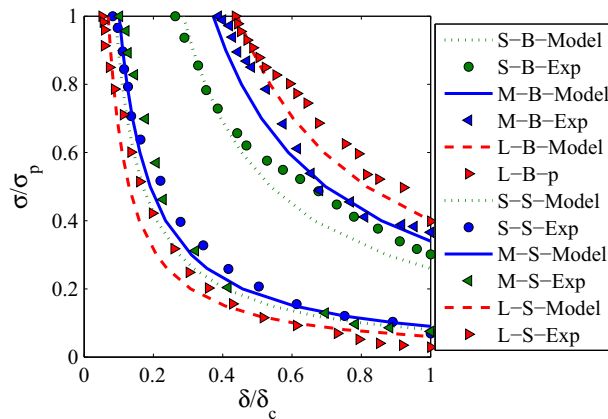


Fig. 4 Comparison of post-peak behavior of normal concrete between proposed model and experiment conducted by Bazant and Xu [21] and Shah [22]. (S/M/L–B/S–Exp/Model stands for Small/Medium/Large–Bazant and Xu/ Shah–Experiment/Model)

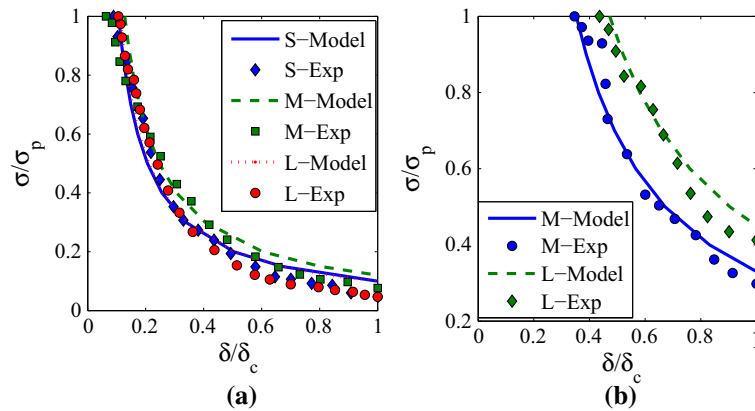


Fig. 5 Comparison of post-peak behavior of high-strength concrete between proposed model and experiment **a** Prasad and Sagar [23] and **b** Gettu et al. [24] (*S* small, *M* medium and *L* large)

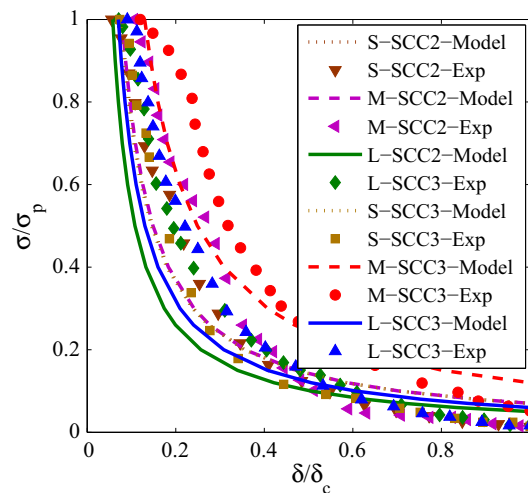


Fig. 6 Comparison of post-peak behavior of self-compacting concrete (SCC) between proposed model and experiment [25] (*S* small, *M* medium and *L* large)

or that of Shah [22]. It is seen that the post-peak response drops sharply for Shah's concrete in comparison with the ones tested by Bazant and Xu. This is due to the different mix proportions of the ingredients used in the preparation of the normal concrete as shown in Table 2. This fact is reflected in the proposed model through the critical microcrack length which depends on the mix properties of the concrete and hence the model is able to predict the experimental response well. In Fig. 5, the results of the proposed model and the experiments on high-strength concrete are presented. In the legend, the letters *S*, *M* and *L* stand for small, medium and large specimens, respectively. Although similar ingredients are used by Prasad and Sagar [23] and Gettu et al. [24] in the preparation of high-strength concrete, the post-peak response is different due to different mix proportions. It is seen that the proposed model is able to capture this effect including those of size. In Fig. 6, the results of self-compacting concrete (SCC) with different mineral additives such as fly ash (SCC2) and fly ash plus silica fume (SCC3) for small (*S*), medium (*M*) and large (*L*) beams are shown. It may be noted that the SCC has a higher powder content when compared to normal- or high-strength concrete. As seen from this figure, the proposed model is able to capture the post-peak response well.

The post-peak softening behavior exhibited by quasi-brittle cementitious materials can be considered to be a material property depicting the energy required to fracture the concrete ligament and is known as the fracture energy. It is well known that this behavior is attributed to the formation of the fracture process zone (FPZ) consisting of microcracks wherein different toughening mechanisms occur, as explained earlier. The properties of the FPZ depend on the mix proportion and size of the ingredients used in the preparation of the concrete. The proposed model is seen to capture the effects of size and the mix proportions well thereby making it robust

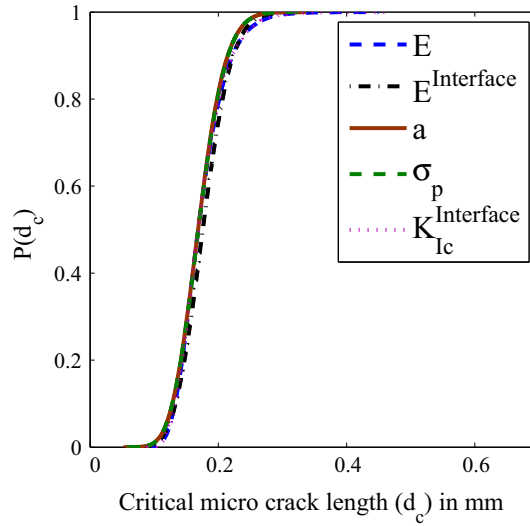


Fig. 7 Probability distribution curves of the critical microcrack length (d_c) for different random variables

and superior to other models available in the literature. The proposed model can thus be used to model the crack tip toughening mechanisms and would be very useful in predicting the fatigue life of different concrete mixes.

9 Sensitivity analysis

In this study, the fracture toughness of the interface, elastic modulus of the interface, elastic modulus of concrete, the macrocrack length and the peak stress are considered as random variables. The probability distribution as well as the statistical properties of the random variables considered in this study are listed in Table 4. Since all the random variables are positive definite, their distribution are taken to be lognormal. The standard deviation of all random variables are taken as ten percent of their corresponding mean values. The mean value of each variable is taken from the experimental data reported by Bazant and Xu [21]. The geometric factors $g_2(\frac{a_c}{b})$ and $g_3(\frac{x}{a_c}, \frac{a_c}{b})$ are computed as 1.8 and 0.1 and it is found to be approximately the same for all specimens.

Using statistical data, ensembles of 50,000 values of each random variable are generated. The values of critical microcrack length (d_c) is simulated six times (as six variables are considered), keeping one of the six independent variable as random at a time and others at their mean value. For all the six cases, a cumulative probability distribution (CDF) is plotted for the critical microcrack length (d_c) as in Fig. 7. The parameter corresponding to the curve with the least slope would be the most sensitive one. As seen from this figure, the elastic modulus of concrete and the fracture toughness of the interface are the most sensitive parameters in the determination of the critical microcrack length.

The coefficient of sensitivity (C_s) is computed to quantify the sensitivity of each parameter and is evaluated using

$$C_{s_i} = 100 \frac{C_{v_i}^2}{C_v} \quad (36)$$

where C_{v_i} is the coefficient of variation of the dependent variable when i th independent variable is considered as random with all others at their mean value and C_v is the coefficient of variation when all independent variables are taken as random.

The results of the coefficient of sensitivity are shown in Table 4. The same results as obtained from the cumulative probability distribution of Fig. 7 are obtained here too indicating that the elastic modulus of concrete and the fracture toughness of the interface are the most sensitive parameters.

Table 4 Statistical parameters used and the results obtained in sensitivity analysis

Parameters	Units	Distribution	Mean μ	Standard deviation σ	Coefficient of sensitivity C_s
E	N/mm ²	Lognormal	27,120	2712	20.5
$K_{IC}^{Interface}$	MPa \sqrt{mm}	Lognormal	12.45	1.245	20.3
a	mm	Lognormal	15.58	1.558	17.8
$E^{Interface}$	N/mm ²	Lognormal	5488.7	548.87	17.8
σ_p	N/mm ²	Lognormal	4.75	0.475	17.7

10 Conclusions

In this study, an analytical model to determine the post-peak behavior of concrete is proposed and validated using a multiscale approach. A critical microcrack length parameter is defined and an expression is derived by analyzing the crack opening displacement at micro- and macroscales. The critical microcrack length is further used in developing a fracture model for plain concrete to study the post-peak behavior. The proposed multiscale fracture model is validated using available experimental data. It is seen that the proposed fracture model predicts the post-peak response of normal strength concrete, high-strength concrete and self-consolidating concrete very well. For a particular mix of concrete, the ratio of critical microcrack length to the specimen depth is found to be constant and could be used as a material property. Through a deterministic sensitivity analysis, it is found that the fracture toughness of the interface and elastic modulus of concrete are the most sensitive parameters influencing its post-peak behavior.

References

- Maso, J.: Interfacial Transition Zone in Concrete, RILEM Report, vol. 11. CRC Press, London (2004)
- Scrivener, K.L., Crumie, A.K., Laugesen, P.: The interfacial transition zone (ITZ) between cement paste and aggregate in concrete. *Interface Sci.* **12**(4), 411–421 (2004)
- Ollivier, J., Maso, J., Bourdette, B.: Interfacial transition zone in concrete. *Adv. Cem. Based Mater.* **2**(1), 30–38 (1995)
- Mihai, I.C., Jefferson, A.D.: A material model for cementitious composite materials with an exterior point eshelby microcrack initiation criterion. *Int. J. Solids Struct.* **48**(24), 3312–3325 (2011)
- Buyukozturk, O., Nilson, A.H., Slate, F.O.: Deformation and fracture of particulate composite. *J. Eng. Mech. Div.* **98**(3), 581–593 (1972)
- Liu, T.C., Nilson, A.H., Floyd, F.O.S.: Stress–strain response and fracture of concrete in uniaxial and biaxial compression. In: *ACI Journal Proceedings*, vol. 69, pp. 291–295. ACI (1972)
- Struble, L., Skalny, J., Mindess, S.: A review of the cement–aggregate bond. *Cem. Concr. Res.* **10**(2), 277–286 (1980)
- Bentur, A., Mindess, S.: The effect of concrete strength on crack patterns. *Cem. Concr. Res.* **16**(1), 59–66 (1986)
- Horii, H., Shin, H.C., Pallewatta, T.M.: Mechanism of fatigue crack growth in concrete. *Cem. Concr. Compos.* **14**(2), 83–89 (1992)
- Nirmalendran, S., Horii, H.: Analytical modeling of microcracking and bridging in the fracture of quasi-brittle materials. *J. Mech. Phys. Solids* **40**(4), 863–886 (1992)
- Mindess, S.: Mechanical properties of the interfacial transition zone: a review. *ACI Spec. Publ.* **156**, 1–10 (1995)
- Van Mier, J., Vervuurt, A.: Numerical analysis of interface fracture in concrete using a lattice-type fracture model. *Int. J. Damage Mech.* **6**(4), 408–432 (1997)
- Prokopski, G., Halbiniak, J.: Interfacial transition zone in cementitious materials. *Cem. Concr. Res.* **30**(4), 579–583 (2000)
- Shah, S.P., Swartz, S.E., Ouyang, C.: *Fracture Mechanics of Concrete: Applications of Fracture Mechanics to Concrete, Rock and Other Quasi-Brittle Materials*. Wiley, New York (1995)
- Prado, E., Van Mier, J.: Effect of particle structure on mode I fracture process in concrete. *Eng. Fract. Mech.* **70**(14), 1793–1807 (2003)
- Sun, C.T., Jin, Z.H.: *Fracture Mechanics*. Elsevier, Amsterdam (2012)
- Hillemeier, B., Hilsdorf, H.: Fracture mechanics studies on concrete compounds. *Cem. Concr. Res.* **7**(5), 523–535 (1977)
- Huang, J., Li, V.: A meso-mechanical model of the tensile behavior of concrete. Part II: modelling of post-peak tension softening behavior. *Composites* **20**(4), 370–378 (1989)
- Yang, C.: Effect of the transition zone on the elastic moduli of mortar. *Cem. Concr. Res.* **28**(5), 727–736 (1998)
- Hashin, Z.: The elastic moduli of heterogeneous materials. *J. Appl. Mech.* **29**(1), 143–150 (1962)
- Bazant, Z.P., Xu, K.: Size effect in fatigue fracture of concrete. *ACI Mater. J.* **88**(4), 390–399 (1991)
- Shah, S.G., Chandra Kishen, J.M.: Fracture properties of concrete–concrete interfaces using digital image correlation. *Exp. Mech.* **51**(3), 303–313 (2011)

-
23. Raghu Prasad, B.K., Vidya Sagar, R.: Relationship between AE energy and fracture energy of plain concrete beams: experimental study. *J. Mater. Civ. Eng.* **20**(3), 212–220 (2008)
 24. Gettu, R., Bazant, Z.P., Karr, M.E.: Fracture properties and brittleness of high-strength concrete. *ACI Mater. J.* **87**(6), 608–618 (1990)
 25. Hemalatha, T., Ramaswamy, A., Chandra Kishen, J.M.: Simplified mixture design for production of self-consolidating concrete. *ACI Mater. J.* **112**(2), 277–286 (2015)
 26. Mobasher, B., Stang, H., Shah, S.: Microcracking in fiber reinforced concrete. *Cem. Concr. Res.* **20**(5), 665–676 (1990)